Journal of Telecommunication, Electronic and Computer Engineering
ISSN: 2180 – 1843 e-ISSN: 2289-8131 Vol. 18 No. 2 (2026) 35-44
jtec.utem.edu.my
DOI: https://doi.org/10.54554/jtec.2026.18.02.005

Alternative Signal Waveform Models for Advanced Interference Mitigation in 5G New Radio Systems

Zakka Augustine[1*], Gambo Danasabe[2], Franklin Chibueze Njoku[1], Jerry Raymond[1], Magaji Musa Marcus[3], Stella Ngozi Obiahu[4]
[1]*Department of Telecommunications Engineering, Faculty of Ground Engineering, Air Force Institute of Technology, Kaduna 800282, Nigeria.*
[2] *Department of Electrical Electronics Engineering, Faculty of Ground Engineering, Air Force Institute of Technology, Kaduna, Nigeria.*
[3] *Department of Cyber Security, Faculty of Computing, Federal University of Applied Sciences, Kachia, Nigeria.*
[4] *Department of Control Engineering, Faculty of Engineering, Ahmadu Bello University, Zaria, Nigeria.*

Article Info

Article history:
Received Mar 14th, 2026
Revised May 6th, 2026
Accepted Jun 3rd, 2026
Published Jun 30th, 2026

Index Terms:
Adjacent Channel Interference
Advanced Interference Mitigation
Inter-Channel Interference
Inter-Symbol Interference

Abstract

The need for alternative signal waveforms capable of effectively mitigating interference and increasing transmission efficiency has remained a major challenge for Fifth Generation (5G) New Radio (NR) systems. To address this challenge, this research developed two modified waveforms by integrating Kaiser and Dolph-Chebyshev window algorithms in a programmable Closed Loop Transfer Function (CLTF) digital module for a Hanning-induced Filtered-Orthogonal Frequency Division Multiplexing (F-OFDM) waveform. This resulted in two alternative waveforms: Hanning-Kaiser Window-induced Filtered Orthogonal Frequency Division Multiplexing (HKW-Induced F-OFDM) waveform and Hanning-Dolph Window-induced Filtered Orthogonal Frequency Division Multiplexing (HDW-Induced F-OFDM) waveform. Simulation results obtained at a 120 kHz Subcarrier Spacing (SCS) showed the HKW-induced F-OFDM waveform achieved Advanced Interference Mitigation (AIM) levels of -25.22 dBm for Adjacent Channel Interference (ACI), -40.05 dBm for Inter-Symbol Interference (ISI), and -53.70 dBm for Inter-Channel Interference (ICI), corresponding to improvements of 22.73%, 24.84%, and 28.49%, respectively, over the conventional HW-induced F-OFDM waveform. Similarly, the HDW-induced F-OFDM waveform achieved AIM levels of -30.02 dBm for ACI, -38.52 dBm for ISI, and -51.17 dBm for ICI, corresponding to improvements of 46.08%, 20.07%, and 22.44% , respectively over the conventional HW-induced F-OFDM waveform. The two proposed waveforms also demonstrated the capability to improve bandwidth utilization and spectral efficiency, thereby meeting the stringent requirements of Frequency Range 2 (FR2/mmWave) deployments ($> 24.25\,GHz$) through effective interference mitigation. This capability was further demonstrated by their scalability in supporting 5G NR numerologies of 0 to 3.

This is an open access article under the CC BY-NC-ND 4.0 license.

*Corresponding Author: zax.austen@yahoo.com

I. INTRODUCTION

Filtering and windowing techniques are among the key performance indicators required to achieve high Spectral Efficiency (SE) in wireless waveform modification [1]. They are widely used to sufficiently mitigate interference and support asynchronous transmission, as stipulated by the Third Generation Partnership Project (3GPP) Fifth Generation (5G) New Radio (NR) objectives. Interference anomalies often result in the underutilization of available radio spectrum resources [2]. To achieve efficient spectral filtering for Advanced Interference Mitigation (AIM), this research adopts an augmented filter response approach. Digital filters are designed to discriminate a desired frequency or frequency band from a signal containing both wanted and unwanted components [3],[4]. These unwanted components are typically caused by interference or noise, which degrade signal quality and adversely affect wireless communication performance [5].

Digital filters used in waveform development are broadly classified into two categories: Finite Impulse Response (FIR) and Infinite Impulse Response (IIR) filters [6]. This research focuses on the FIR filter function, specifically the Windowed-Sinc filter, to modify a Filtered-Orthogonal Frequency Division Multiplexing (F-OFDM) waveform. F-OFDM is an Orthogonal Multiple Access (OMA) waveform proposed for fifth-generation (5G) wireless telecommunication systems to support massive connectivity and flexible spectrum allocation through sub-band filtering

[7]. Unlike Non-Orthogonal Multiple Access (NOMA), which primarily improves spectral utilization through power-domain multiplexing, OMA achieves spectral efficiency by allocating orthogonal frequency, time, or code resources [8]. This provides an alternative and advanced waveform architecture for 5G NR systems, with enhanced capability for mitigating interference.

Despite its advantages, F-OFDM suffers from the reintroduction of Adjacent Channel Interference (ACI), Inter-Carrier Interference (ICI), and Inter-Symbol Interference (ISI), following the removal of the Cyclic Prefix (CP) at the receiver side of a wireless transceiver [9]. To address these limitations, this work proposes an AIM scheme, which employs the systematic design and implementation of a programmable of a programmable Closed Loop Transfer Function (CLTF) module integrated into the F-OFDM receiver. The proposed CLTF module is conceptually analogous to the Cyclic Prefix-Orthogonal Frequency Division Multiplexing (CP-OFDM) technique for interference mitigation, in which a portion of the symbol suffix is copied and appended as a prefix prior to transmission [10]. This principle enables CP-OFDM to provide effective interference mitigation and robustness against multipath propagation. However, the insertion of the cyclic prefix introduces bandwidth overhead, resulting in reduced spectral efficiency, increased transmission time, and higher power consumption [11],[12]. Nevertheless, CP-OFDM remains attractive because of its robustness against multipath propagation and its relatively low sensitivity to timing errors [13],[14].

In the proposed approach, unwanted bit codes identified during the channel estimation stage of a Hanning Windowed (HW)-based F-OFDM receiver are extracted and redirected to an alternative filtering path employing either the Kaiser Windowed (KW) or Dolph Windowed (DW) filters within the Closed-Loop Transfer Function (CLTF) module. These signals are subsequently post-filtered using the interference suppression capability of the FIR digital filters. After the interference has been reduced to the desired threshold through the adaptive KW- or DW-based filters, the resulting filtered signal is fed back to the input section of the receiver through the programmable CLTF module. The feedback signal complement any residual error pulses while providing the required timing synchronization to effectively suppress ACI, ICI, and ISI. Finally, the processed waveforms are passed through the channel estimation stage for demodulation, ensuring that only waveforms satisfying the required signal quality threshold are recovered. This approach facilitates efficient network slicing in accordance with the requirements of 5G NR and beyond [2].

In this work, the modified waveforms are intended deployment using 60 kHz and 120 kHz Subcarrier Spacings (SCSs) corresponding to higher 5G numerologies and beyond. This is aimed at supporting transmission within the Frequency Range 2 (FR2) spectrum of 24.52 GHz - 52.60 GHz [15]. Experimental studies have shown that higher SCS values enable more efficient data transmission [16]. For example, smartphones operating with numerologies 2 and 3 exhibit lower timing jitter, making them well-suited for bidirectional communication [17]. However, the adoption of higher SCS values to mitigate interference may also result in spectrum underutilization and network redundancies. Consequently, Software Defined Radio (SDR), Cognitive Radio (CR), and Machine Learning (ML) techniques are proposed as promising technique solutions for maximizing the utilization of these underutilized spectral resources while improving system scalability [18]. This constitutes one of the key recommendations of this work for meeting the increasing data rate requirements of 3GPP 5G NR and future wireless communication systems.

The novelty of this research lies in the integration of adaptive filtering techniques into a programmable CLTF module that generates a complementary feedback signal for waveform modification, thereby enhancing interference mitigation in higher operating frequencies. The fundamental innovation of combining Hanning-, Kaiser-, and Dolph-windowing techniques in a CLTF-enhanced F-OFDM receiver lies in achieving adaptive, real-time control of spectrum leakage while preserving waveform orthogonality and effectively balancing high spectral efficiency with robust asynchronization operation for 5G and emerging 6G communication systems. To the best of the authors' knowledge, this integrated CLTF-assisted adaptive windowing framework has not been comprehensively investigated in the existing literature. Rather than creating an entirely new waveform, this research modifies an existing waveform architecture to satisfy the specific interference mitigation and spectral efficiency measurements of next-generation wireless communication systems.

II. THEORETICAL BACKGROUND

This section presents the theoretical background of this research, which include the filter design and its realization. It also presents the conceptual framework adopted for the generation of the proposed alternative waveforms for AIM, together with the corresponding signal decision threshold. The filter design approach adopted in this work the windowing method because signal filtering and windowing are among the key techniques required for waveform modification in 5G New Radio (NR) systems [1]. In this work, waveform modification is achieved using a programmable CLTF module incorporated into an F-OFDM waveform. The proposed CLTF module adopted in this work is a programmable memory system that possesses prior knowledge and the ability to autonomously adjust the received signal information based on the characteristics of the transmitted signal information.

The Hanning, Kaiser, and Dolph-Chebyshev windows are employed in the design of the FIR filters used in this research. They are selected to achieve control of spectral leakage, excessive power, Doppler shift, frequency selectivity, unnecessary power consumption, and filter-tail distortion. Additionally, the Kaiser-window-based and Dolph-window-based FIR filters are incorporated into the feedback path of the CLTF module integrated with an F-OFDM receiver. These FIR filters serve as adaptive interference mitigation components for modern wireless communication systems [17]. With this systematic arrangement and timing, the proposed framework generates an alternative waveform capable of mitigating ACI, ICI and ISI, thereby improving the overall efficiency of the wireless communication system.

A. Hanning Windowing Filter

The Hanning window (HW) is one of the most widely used window functions for sub-band filtering to achieve asynchronous waveforms. It belongs to the family of generalized cosine windows [19]. It has the advantage of

generating lower side lobes, which helps mitigate Out-of-Band Emission (OoBE) and reduce the Peak-to-Average Power Ratio (PAPR) in orthogonal transmission systems [20]. These characteristics make it suitable for deployment at both the transmitter and receiver of a wireless communication system. Accordingly, it is used in this work to generate the Hanning-window (HW)-based FIR filter used in the proposed waveform modification framework. The Hanning window (HW) coefficient is expressed as (1) as computed in [21]:

$$W_{HW}^{*}(n) = 0.5[1 - \cos\left(\frac{2\pi n}{N_W}\right)]^{\alpha} \quad (1)$$

where, $N_W = M_f - 1$, is the length of the window and α is the roll-off (window shaping) factor.

To obtain the HW-based FIR filter, $F_{HW}^{*}(n)$ for effective F-OFDM transmitter/receiver filtering, the ideal low-pass filter sinc transfer function, $h_d(n)$ is multiplied with the HW function, $W_{HW}^{*}(n)$, as given in [22]:

$$F_{HW}^{*}(n) = h_d(n)W_{HW}^{*}(n) \quad (2)$$

The received F-OFDM waveform is then matched with the transmitted waveform through time-domain convolution to obtain the asynchronous received signal, $R_{in}(n)$, expressed as (3):

$$R_{in}(n) = R(s)^{*}F_{HW}^{*}(-n) \quad (3)$$

where, $R(s)^{*}$ denotes the received signal impulse response across subcarriers, while $F_{HW}^{*}(-n)$ represents the time-reversed FIR spectrum-shaping filter applied at the receiver tail.

B. Kaiser Windowing Filter

The Kaiser Window (KW) is widely employed in FIR filter design because of its excellent capability for controlling spectral leakage and improving spectral concentration [23]. For a window containing N_W samples, the Kaiser window function $W_{KW}^{*}(n)$, represented by Equation 4 is defined by the attenuation function, β. Equations (4) - (8) are used to compute the coefficient of the KW. The KW function is given for $0 \leq n \leq M_f = 1$ in [22], in correspondence to the filter taps, N_f:

$$W_{KW}^{*}(n) = \frac{lo[\beta\sqrt{1-\left(1-\frac{2n}{N_W}-1\right)^2}]}{lo[\beta]}, \quad (4)$$

where: $\beta = \pi\alpha$ is the attenuation function, consisting of the waveform phase, π and the roll-off factor, α, while $lo[.]$ denotes the modified zero-order Bessel function given by [24] as:

$$lo[\beta] = 1 + \sum_{k=1}^{\infty}[\frac{(\beta/2)^2}{k!}] \quad (5)$$

and,

$$\beta = \begin{cases} 0.1102(A_s - 8.7), & A_s \geq 50 \\ 0.5842(A_s - 21)^{0.3} + 0.07886(A_s - 21), & 21 < A_s < 50 \end{cases} \quad (6)$$

where, A_s denotes the minimum stop-band attenuation and β is the parameter that depends on N_W, and is chosen to yield various transition widths and near optimum stop-band attenuation. The pertinent design parameters are: w_s and A_s, which are obtained from the following relationships of the normal transition width [25]:

$$\Delta_{\omega} = \frac{w_s - w_p}{2\pi} \quad (7)$$

where, $w_s - w_p$ is the width of the transition band, with w_s denoting the width of the stop-band and w_p representing the width of the pass-band. w_s and w_p are also termed corner frequencies.

The filter length, $N_f = M_f - 1$ is also determined by selecting the lowest odd value of N_f that would satisfy the inequality [26]:

$$N_f \geq \frac{\omega_{\text{samp}}D}{\Delta\omega} + 1 \quad (8)$$

where the parameter D, is determined using the expression:

$$D = \begin{cases} 0.9222, & A_s \leq 21 \\ \frac{A_s - 7.95}{14.36\Delta f}, & A_s > 21 \end{cases} \quad (9)$$

and, ω_{samp} is the normalized sampling frequency and $\Delta\omega$ is the transition width.

However, windows are analyzed in the frequency domain to compare and classify them in terms of their spectral characteristics. The frequency spectrum of a window is obtained in (10):

$$W(e^{jwt}) = e^{-jw(N_W-1)T/2}W_0(e^{jwT}) \quad (10)$$

where,

$W_0(e^{jwT})$ is the amplitude function.
$N_W = M_f - 1$ denotes the window length, which is the same with the filter length, N_f used.
T corresponds to the interval between samples.

This is useful when plotting the normalized amplitude spectrum of the window.

To obtain the desired attenuated waveform, the Kaiser-window-based FIR filture, $F_{KW}^{*}(n)$ is applied to the distorted F-OFDM signal containing ACI, ICI, and ISI to filter out the interference signal pulses from the useful ones. The corresponding filtered signal, $R_{KW}(n)$ is expressed as

$$R_{KW}(n) = Z_n(n)^{*}F_{KW}^{*}(n) \quad (11)$$

where, $F_{KW}^{*}(n)$ is the Kaiser-window-based FIR filter obtained by multiplying the ideal low-pass transfer function, $h_d(n)$ with KW functions, $W_{KW}^{*}(n)$, and $Z_2(n)$ represents the undesired F-OFDM signal that are contaminated with ACI, ICI, and ISI.

C. Dolph-Chebyshev Windowing Filter

The Dolph-Chebyshev window (DW) is well known for its ability to produce a wide main lobe (wideband) while providing effective control of spectral aliasing. The zero-phase DW function, $W_{DW}^{*}(n)$ expressed in (12), is defined in terms of its real-valued discrete Fourier transform for $0 \leq n \leq M_f - 1$ [23].

$$W_{DW}^{*}(n) = \frac{\cos(N\cos^{-1}\left[\beta\cos\left(\frac{\pi k}{N_W}\right)\right])}{\cosh[N\cosh^{-1}(\beta)]}, \quad (12)$$

$$\text{where, } \beta = \cosh[\tfrac{1}{N}cosh^{-1}(10^{\alpha})], \quad (13)$$

The value of α determines and influences the side-lobes attenuation. Its normal window function, $w_0(n)$ is presented in (14) as in [19].

$$w_0(n) = w_0(n - \tfrac{N_W}{2}), \quad (14)$$

Similar to (11), the Dolph-window-based FIR filter, $F_{DW}^{*}(n)$, is applied to the distorted F-OFDM signal containing ACI, ICI, and ISI to separate the unwanted signal components from the wanted ones. The corresponding filtered signal, R_{DW}(n) is expressed as

$$R_{DCW}(n) = Z_2(n)^{*}F_{DW}^{*}(n) \quad (15)$$

where, $F_{DW}^{*}(n)$ is the Dolph-window-based FIR filter, obtained by multiplying the ideal low-pass transfer function, $h_d(n)$ with DW functions, $W_{DW}^{*}(n)$.

III. RESEARCH METHODOLOGY

This section presents the materials and methods, together with the pictorial and mathematical models, used to realize this research. The operation of the programmable CLTF module, which enhances waveform modification to achieve AIM is clearly demonstrated. The proposed module is incorporated at the receiver side of an F-OFDM wireless system to identify and compensate for signal pulses distorted by interference or deviating from the transmitted signal information. To achieve the desired system efficiency, the seamless integration of the CLTF module with the F-OFDM receiver is demonstrated using a flowchart algorithm.

A. Materials and Method

The successful integration of the CLTF module with the Hanning-induced F-OFDM waveform consists of the folded spectrum-shaping filter, G_1, the demultiplexer unit, $\otimes$, the channel estimation region, G_2, the error control system, β, and the demodulator, $\otimes$. The following steps describe the operating principles of the proposed model.

- The received signal, $R_s(n)$ is reconstructed at the receiver of F-OFDM system after propagating through the fading channel.
- The received signal is prefiltered using the folded spectrum-shaping filter, G_1 to correct anomalies caused by channel noise and multipath propagation.
- The demultiplexer unit, $\otimes$ removes the CP to reduce transmission overhead. Following CP removal, ACI, ICI an ISI become more pronounced and require mitigation to support higher 5G NR frequencies.
- The system gain region, G_2, serves as the channel estimation region, where a decision threshold of 0.5 is established within the range of 0 and 1.
- The decision threshold differentiates between signals corrupted by interference, $Z_2(n)$ and signals with relatively lower interference, $Z_1(n)$.
- The corrupted signal pulses, $Z_2(n)$ are extracted and forwarded to the Kaiser-window-based or Dolph-window-based FIR filter, represented by $H(n)$ for post − filtering or β region containing either the $F_{KW}^{*}(n)$ or $F_{DW}^{*}(n)$ filter. These filters complement the waveform reconstruction process by restoring the distorted signal $Z_2(n)$ in accordance with the transmission bits' standards.
- The filtered signal waveforms, $R_f(n)$ is subsequently fed back to compensate for the received signal pulses identified as interfered. The corrected signal is subsequently verified through the system gain region, G_2 , before demodulation.
- The final alternative waveforms are obtained as HKW-induced F-OFDM and HDW-induced F-OFDM waveforms.

B. System Modeling

Figure 1 presents a schematic workflow diagram of the proposed methodology for realizing the programmable CLTF module used for waveform modification. In this work, the HKW-induced F-OFDM waveform is employed to satisfy both FR1 and FR2 waveform requirements, whereas the HDW-induced F-OFDM waveform is used to satisfy FR2 and future FR-A waveform requirements. This design is intended to satisfy the waveform development requirements specified in the International Telecommunication Union (ITU) and 3GPP NR release 15, 16, 17, and 18.

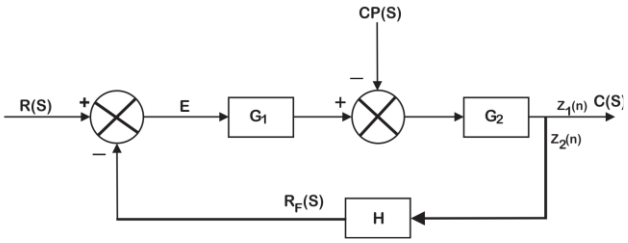


Figure 1. A CLTF Feedback Module

The received signal response, $R(s)$ after propagating through the fading channel is expressed as (16) following [2]:

$$R_s(n) = [h(n)S(n) + W(n)] \quad (16)$$

where:

$h(n)$ represents the channel impulse response.
$S(n)$ represents the F-OFDM information carrying symbols.
$W(n)$ is the Additive White Gaussian Noise (AWGN) channel, which is a function of the type of fading channel experienced.

The waveform representation of (16), before the introduction of the folded spectrum-shaping filter, is expressed as:

$$y_k(n) = \tfrac{1}{K}\textstyle\sum_{i=0}^{I}\sum_{n=0}^{N-1} R_k(n)e^{\frac{j2\pi}{N}} \quad (17)$$

where k denotes the waveform sample coefficient.

In the CLTF module shown in Figure 1, G_1 represents the condition of the received signal information at the folded version of an asynchronous spectrum shaping filter,

$F^*_{HW}(-n)$ of the F-OFDM system described in (3). It is defined as the error factor regulator, E as:

$$G_1 = E = R_s(n) - R_f(n)Z_1(n) \quad (18)$$

where, $R_f(n)$ is the alternative filtered signals and $Z_1(n)$ represents to the CLTF baseband samples gained across the subcarriers.

To derive the CLTF gain, the *CP* overhead is first removed in the channel estimation region, G_2, to improve system efficiency. This process is represented in the CLTF module in Figure 1 as:

$$G_2 = G_1 - CP \quad (19)$$

The alternative filtered signal response is then expressed as:

$$R_f(n) = H(n)Z_2(n) \quad (20)$$

Accordingly, the conventional CLTF model for AIM signal waveform modification is expressed as:

$$\frac{Z_1(\mathrm{n})}{R_S(n)} = \frac{G_2}{1+G_2R_f(\mathrm{n})} \quad (21)$$

Substituting (19) and (20) into (21), the baseband signal samples gain, $Z_1(n)$ across a wireless system yield:

$$Z_1(n) = \frac{[G_1 - \mathrm{CP}]R_S(n)}{1+[G_1 - \mathrm{CP}]R_f(\mathrm{n})} \quad (22)$$

where $R_f(n)$ represents either $R_{KW}(n)$ or $R_{DW}(n)$, which are the alternative filtered signals generated from (11) and (15) respectively.

Similarly, the CLTF baseband samples gain, $Z_{HKW}(\mathrm{n})$ containing the payload and pilot data modified by (11) is expressed as:

$$Z_{HKW}(\mathrm{n}) = \frac{[F^*_{HW}(-n) - \mathrm{CP}]R_S(n)}{1+[F^*_{HW}(-n) - \mathrm{CP}]R_{HKW}(\mathrm{n})} \quad (23)$$

Similarly, the CLTF baseband samples gain, $Z_{HDW}(\mathrm{n})$ containing the payload and pilot data modified by (15) is expressed as:

$$Z_{HDW}(\mathrm{n}) = \frac{[F^*_{HW}(-n) - \mathrm{CP}]R_S(n)}{1+[F^*_{HW}(-n) - \mathrm{CP}]R_{HDW}(\mathrm{n})} \quad (24)$$

Both $Z_{HKW}(\mathrm{n})$ and $Z_{HDW}(\mathrm{n})$ are adaptive systems that autonomously adjust their responses to satisfy different waveform requirements for generic wireless communication applications.

Equations (23) and (24) represent the iterative computations performed within the channel estimation region of the AIM model receiver. After completing these iterations, the desired AIM signal is demodulated to recover the original transmitted information.

Finally, the equivalent waveform representation of (23) and (24) at the receiver's output is expressed in (25). This is achieved by transforming (23) and (24) into their original orthogonally spaced multicarrier form, which is also determined by the system numerology specified for 5G NR, yielding:

$$Y_K(e^{j\omega}) = \frac{K}{A_K}\int_{i=o}^{I}\int_{n=0}^{N-1} Z_k(e^{j\omega})e^{-\frac{j\omega}{N}} \quad (25)$$

where, Z_k denotes the modified AIM waveform obtained from (23) and (24)

IV. RESEARCH ALGORITHM

This section presents the graphical algorithm of a sub-band network architecture considered in this research. The proposes an algorithm that compensates for signal aberrations and transmission bottlenecks commonly observed at the receiver side of a wireless communication system. Previous studies have shown that these bottlenecks are primarily caused by ACI, ICI, and ISI. The compensation process for distorted transmission signal pulses is illustrated in Figure 2.

The algorithm begins with the initialization of the input waveform data in the time domain and proceeds through successive processing stages to generate the output waveform, $y_k(n)$, and its corresponding frequency domain representation, $Y_K(e^{j\omega})$. After the modulation and multiplexing processes, the CP is removed to reduce bandwidth overhead and eliminate transmission redundancies. In a sub-band architecture of this nature, ACI, ICI, and ISI distortions become more pronounced following the removal of the CP.

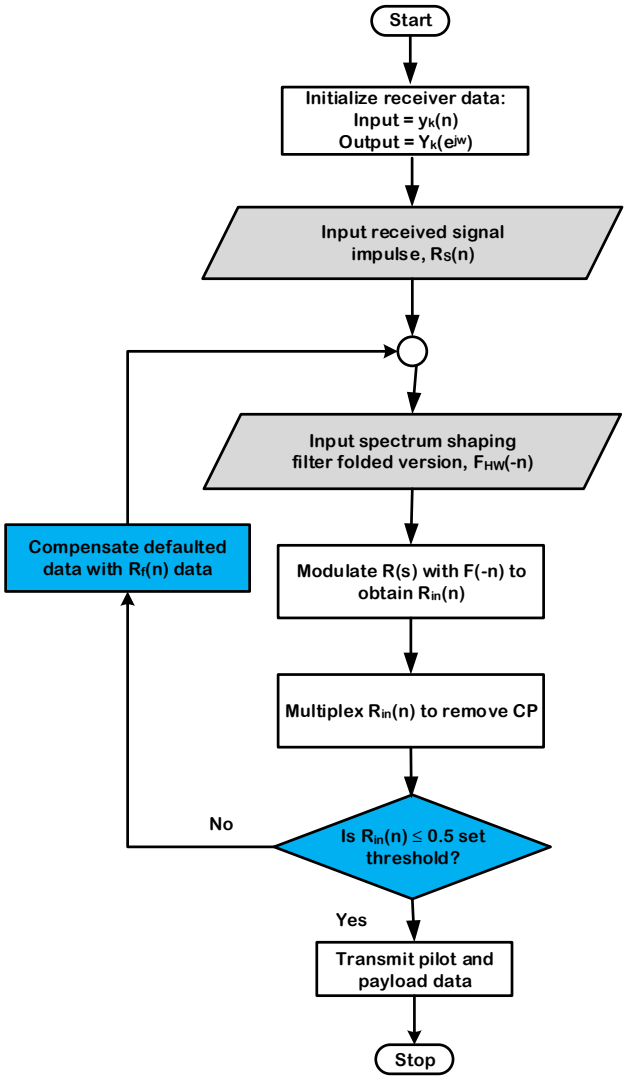


Figure 2. AIM Flow Chart

The CLTF module is a programmable model that differentiates between pilot and payload symbols, as well as wanted and unwanted signal pulses, based on an established threshold of 0.5 within the range of 0 and 1. The data classification is performed using 8-bit symbols mapped according to a 256 QAM modulation scheme. The decision block shown in Figure 2 serves as the channel estimation region, where the received signal pulses are classified as either wanted and unwanted. By dividing each 8-bit symbol into two 4-bit nibbles. Any symbol containing an equal number of 0s and 1s is identified as pilot symbols. For the remaining symbols, those containing more 0s than 1s are classified as wanted signal pulses, whereas those containing more 1s than 0s are classified as unwanted signal pulses. When unwanted signal pulses are detected, the CTLF module activates its adaptive feedback mechanism by utilizing previously stored transmission information to compare and compensate for the detected discrepancy; otherwise, the signal is classified as wanted.

V. RESULTS AND DISCUSSION

The simulations in this research were carried out using the PyCharm Integrated Development Environment (IDE) with Python scripts. The research considered a Cyclic Prefix length of $(1/16)N$, where N is the IFFT/FFT length. A filter length, N_f, of 257 was considered in all cases. The window length, N_W was taken to be the same as the filter length, N_f. The adjustable characteristics of the two windowed filters (KW and DW) employed in this work made it possible to vary their parameters to support the $15\ kHz\ x\ 2^n$ numerology models required for 3GPP 5G NR systems. This was intended to achieve effective interference control, improve system processing time, increase the data rate, enhance throughput scalability, and optimize bandwidth utilization. The simulations were conducted using $60\ kHz$ and $120\ kHz$ Subcarrier Spacings (SCSs) to facilitate effective handover between 5G FR1 and FR2.

Each HW-induced F-OFDM subcarrier symbol contained 8-bit data represented by binary digits 0 and 1. A symbol was classified as wanted if it contained more zeros than ones and unwanted if it contained more ones than zeros. A subcarrier symbol containing 4 bits of zeros and 4 bits of ones was classified as a pilot subcarrier. The research also adopted a decision threshold of 0.5 within the range of 0 and 1. Table 1 summarizes the remaining simulation parameters used in this work.

Table 1
Research Parameters

Parameters	Specifications
Channel Access	F-OFDM
Filter mode	FIR
Window	Hanning, Kaiser, Dolph
Roll-off factor, α	1 for Hanning, variable from 0 to 10 for the adjustable windows.
β	1, 6, 10, 16
ρ	1, -45, -80, -100
FFT size, N	4096
Defected subcarriers, N_d	2016
Number of sub-bands, K	80
Defected Sub-bands,	42
Sub-band bandwidth, M	48
Bits per symbol	8
Bandwidth, BW	100 MHz, 200 MHz
Subcarrier spacing	60 kHz. 120 kHz
Service Numerology	2, 3
Mapping order	256 QAM

A. *Hann, Dolph, and Kaiser Window-Based FIR Filters Frequency Responses*

This section presents the individual frequency responses of the Hann, Dolph, and Kaiser window-induced FIR filters in dBm. As presented in the analysis, the final results were obtained using the Hann-Kaiser Windowed (HKW)-induced F-OFDM and Hanh-Dolph Windowed (HDW)-induced F-OFDM waveforms, which were compared with the conventional Hann Window (HW)-induced F-OFDM waveform in terms of interference mitigation performance.

In a wireless communication system, an IFFT/FFT size of 4096 symbols, with each symbol consisting of 8 bits, represented a considerably large dataset for 5G systems. Due to computational limitations, the dataset was sub-divided into 48 sub-bands, each containing $8-$bit symbols, and subsequently grouped into 12 subcarriers index samples. Processing the entire dataset simultaneously would have resulted in high computational complexity. Therefore, the data were categorized into 80 classes as follows: (1) 0-47, (2) 48-95, …, (80) 4067-4095. The analysis considered the first class (0-47) as the reference because it was the most susceptible to interference compared with the remaining data classes.

Figure 3 presents the frequency response of the Hanning-window-based FIR filter, $F^*_{HW}(n)$. Its roll-off factor was fixed at 1 throughout this work. The results showed that the Hanning window exhibited relatively low side lobes with an attenuation level of approximately -45 dBm. This made the filter effective in controlling spectral leakages, Out-of-Bound Emission (OoBE), and Peak-to-Average Power Ratio (PAPR). These characteristics made the Hanning-window-based FIR filter suitable for deployment at both the transmitter and receiver of a wireless communication system. In this work, the filter was implemented using a $120\ kHz$ Subcarrier Spacing (SCS) with an embedded 257-tap Hanning-window-based FIR filter.

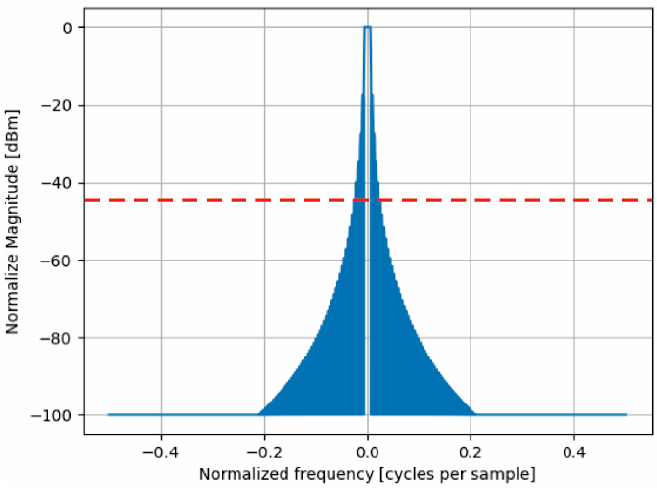
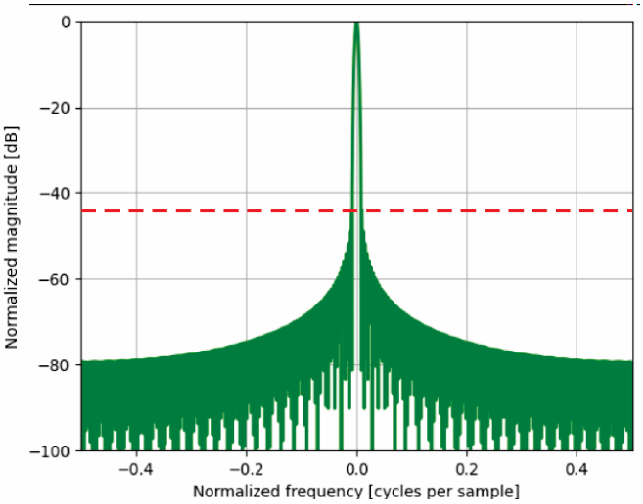


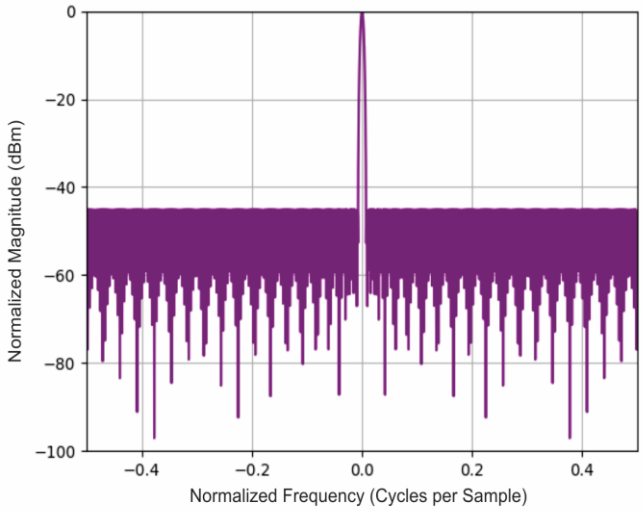
Figure 3. Frequency Response of Hanning-Window-Based FIR Filter

Figures 4 (a) and 4(b) present the individual frequency responses of the Kaiser-window-based and Dolph-window-based FIR filters respectively. It was observed that the Kaiser-window-based FIR filter with $\beta = 6$ performed comparably to the Dolph-window-based FIR filter at an attenuation level of $-45\ dBm$. The attenuation parameter, β, and the pass-band ripple factor, ρ, were continuously varied to obtain the desired FIR filter characteristics for generating the proposed alternative waveforms used for AIM and noise

suppression. The results showed that the Kaiser-window-based FIR filter exhibited a relatively narrow main lobe width with higher transition steepness, making it effective in controlling the main-lobe width friction. In contrast, the Dolph-window-based FIR filter exhibited the widest main lobe and provided superior stop-band attenuation, resulting in better noise suppression, although with lower transition steepness than the Kaiser-window-based FIR filter.



(a) Kaiser Induced Filter Frequency Response at β = 6



(b) Dolph-Chebychev Induced Filter Frequency Response at ρ = -45

Figure 4. Frequency Response of Kaiser-and Dolph-Window- Based FIR Filters

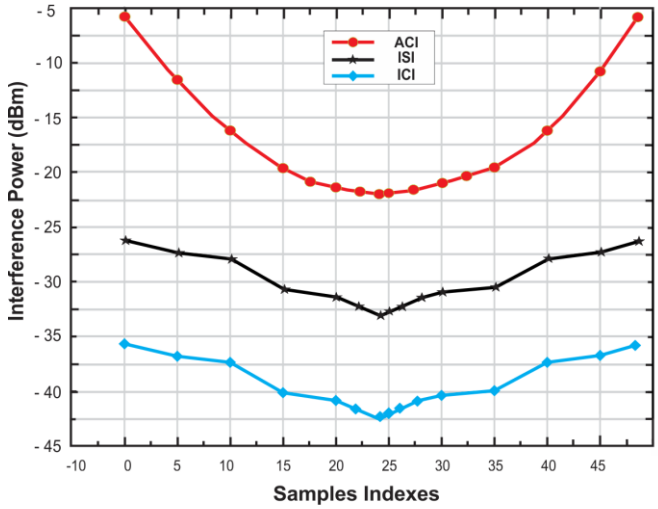
B. Interference Mitigation Results

To avoid complexity in the simulation and data interpretation, this research presented its results using a baseline mathematical model. The sample data were synthesized by the superposition of the 48 sub-band bandwidths into 4 bands, each consisting of 12-sample indices. The average AIM power, I_{AIM} and the baseline value, I_{BV} were determined by dividing the summation of the individual power values, I_{Total} by the number of sample indices, I_{Samp}, as expressed in (26):

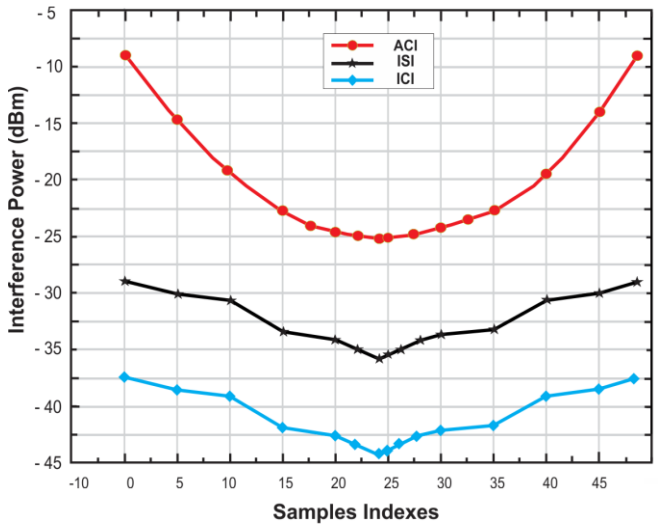
$$I_{AIM/BV} = \frac{\sum_{k=1}^{M} I_{Total}}{I_{Samp}} \quad (26)$$

The Performance Improvement (PI) of the proposed HKW-induced F-OFDM and HDW-induced F-OFDM waveforms was compared with that of the conventional HW-induced F-OFDM waveform for AIM analysis. The percentage improvement of ACI, ISI, and ICI mitigation was determined, as given in (27):

$$PI = \frac{I_{AIM} - I_{BV}}{I_{BV}} \; x \; 100\% \quad (27)$$



(a) Interference Power Detection in 60 kHz SCS using Hanning Induced F-OFDM



(b) Interference Power Detection in 120 kHz SCS using Hanning Induced F-OFDM

Figure 5. Hanning-Induced F-OFDM Interference Power Mitigation with Subcarrier Bandwidth, $M = 48$ at (a) $\Delta_f = 60\ kHz$ and (b) $\Delta_f = 120\ kHz$.

Figure 5 presents the simulated interference power mitigation results for ACI, ISI, and ICI using HW-induced F-OFDM waveform with different SCSs. The interfered waveforms were analyzed after the removal of the CP. The same CP length was adopted for both 60 kHz and 120 kHz SCS to facilitate a fair comparison of the scalability of the HW-induced F-OFDM waveform. It was observed that the ICI sensitivity level of $-41.79\ dBm$ achieved at 120 kHz SCS provided better interference mitigation than all the other interference components. In contrast, the ACI sensitivity level of $-20.55\ dBm$ remained the least suppressed. At 60 kHz SCS, the ACI level further degraded to $-16.95\ dB$.

This behavior was attributed to the relationship between the SCS rate and CP length.

At $120\ kHz$ SCS, the average ACI level of $-20.55\ dBm$ achieved a performance improvement of 21.23% over its baseline value. This improvement was greater than those obtained for ISI ($-32.08\ dBm$) and ICI ($-41.79\ dBm$), owing to the improved asynchronous operation among the sub-bands. Likewise, the results showed that ISI had a greater impact on the system performance than ICI under the operating conditions investigated.

Table 2 presents the comparison of interference mitigation achieved by the HW-induced F-OFDM waveform at $60\ kHz$ and $120\ kHz$ SCS. It was observed that the HW-induced F-OFDM waveform operating at $120\ kHz$ SCS achieved better interference mitigation, recording $-20.55\ dBm$ for ACI, $-32.08\ dBm$ for ISI, and $-41.79\ dBm$ for ICI, compared with $-16.95\ dBm$ for ACI, $-29.45\ dBm$ for ISI, and $-39.25\ dBm$ for ICI, respectively, at $60\ kHz$ SCS. Consequently, the HW-induced F-OFDM waveform operating at $120\ kHz$ SCS achieved performance improvements of 21.23% for ACI, 8.93% for ISI, and 6.47% for ICI over the $60\ kHz$ SCS configuration.

However, it was observed from the interference power levels expressed in dBm that the HW-induced F-OFDM waveform did not satisfy the estimated threshold required for effective 5G FR2 transmission and, therefore was more suitable for 5G FR1 operation. This finding demonstrated the limitation of the HW-induced F-OFDM waveform in terms of scalability toward higher-frequency applications. Furthermore, it was observed that the performance of the HW-induced F-OFDM waveform at $120\ kHz$ SCS degraded as the data size increased, compared with its performance at $60\ kHz$ SCS. These observations motivated the development of the proposed AIM model, which was designed to extend the interference mitigation capability beyond the conventional 5G FR1 operating requirements.

Table 2
Interference Power Mitigation of HW-Induced F-OFDM at 120 kHz versus 60 kHz SCS

Interference	HW-Induced F-OFDM at 60 kHz SCS	HW-Induced F-OFDM at 120 kHz SCS	Percentage Improvement
ACI Power (dBm)	-16.95	-20.55	21.23%
ISI Power (dBm)	-29.45	-32.08	8.93%
ICI Power (dBm)	-39.25	-41.79	6.47%

Figures 6 and 7 respectively present the simulated interference mitigation results obtained for AIM at $120\ kHz$ SCS using the HKW-induced F-OFDM and HDW-induced F-OFDM waveforms. It was observed from both figures that the HKW-induced F-OFDM waveform achieved better ICI and ISI mitigation, recording $-53.70\ dBm$ and $-40.05\ dBm$, respectively, compared with the HDW-induced F-OFDM waveform, which achieved $-51.17\ dBm$ and $-38.52\ dBm$, respectively. This improvement was attributed to the superior interference suppression capability of the Kaiser-window-based FIR filter, resulting from its effective control of spectral leakage and improved spectral concentration compared with the Dolph-window-based FIR filter. Conversely, the HDW-induced F-OFDM waveform achieved superior ACI mitigation, recording -30.02 dBm compared with $-25.22\ dBm$ achieved by the HKW-induced F-OFDM waveform. This behavior was attributed to the fact that ACI is primarily associated with noise occurring near the edges of the subcarriers.

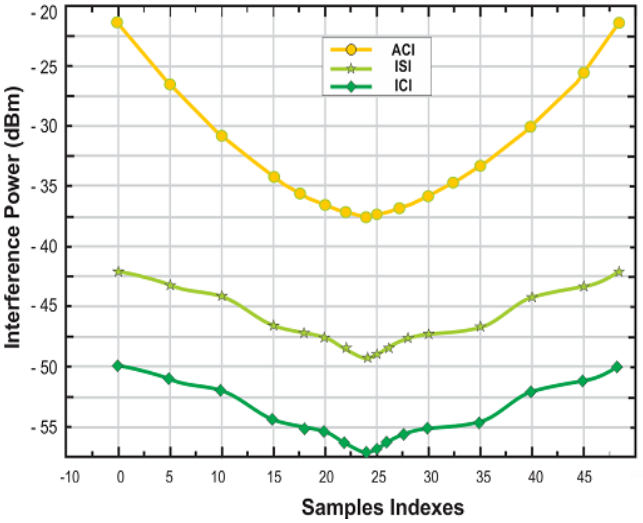


Figure 6. Interference Power Mitigation of the HKW-Induced F-OFDM Waveform at $120\ kHz$ SCS.

Table 3
Interference Power Mitigation of the HKW-Induced F-OFDM Waveform versus the HW-Induced F-OFDM Waveform at 120 kHz SCS.

Interference	HW-Induced F-OFDM at 120 kHz SCS	HKW-Induced F-OFDM at 120 kHz SCS	Percentage Improvement
ACI Power (dBm)	-20.55	-25.22	22.73%
ISI Power (dBm)	-32.08	-40.05	24.84%
ICI Power (dBm)	-41.79	-53.70	28.49%

When the interference mitigation capability of the proposed HKW-induced F-OFDM waveform operating at $120\ kHz$ SCS was compared with that of the conventional HW-induced F-OFDM waveform, as presented in Table 3, it was observed that of the HKW-induced F-OFDM waveform outperformed the conventional HW-induced F-OFDM waveform. The HKW-induced F-OFDM waveform achieved interference power levels of $-25.22\ dBm$ for ACI, $-40.05\ dBm$ for ISI, and $-53.70\ dBm$ for ICI, compared with $-20.55\ dBm$, $-32.08\ dBm$, and $-41.79\ dBm$, respectively, achieved by the conventional HW-induced F-OFDM waveform. Furthermore, the HKW-induced F-OFDM waveform achieved interference mitigation improvements of 22.72% for ACI, 24.84% for ISI, and 28.49% for ICI over the conventional HW-induced F-OFDM waveform.

The superior performance of the HKW-induced F-OFDM waveform was attributed to the adaptive characteristics of the Kaiser-window-induced FIR filter, which provided effective control of spectral leakage and improved spectral concentration. These characteristics enhanced the suppression of ICI and ISI, resulting in better overall interference mitigation while preserving waveform orthogonality.

Similarly, Figure 7 and Table 4 present the interference mitigation performance of the HDW-induced F-OFDM waveform compared with the conventional HW-induced F-OFDM waveform at $120\ kHz$ SCS. The results shows that the HDW-induced F-OFDM waveform achieved interference power levels of $-30.02\ dBm$ for ACI, $-38.52\ dBm$ for ISI, and $-51.17\ dBm$ for ICI, compared with $-20.55\ dBm$ for ACI, $-32.08\ dBm$ for ISI, and $-41.79\ dBm$ for ICI achieved by the conventional HW-induced F-OFDM waveform. Furthermore, the HDW-induced F-OFDM

waveform achieved performance improvements of 46.08% for ACI, 20.07% for ISI, and 22.44% for ICI over the conventional HW-induced F-OFDM waveform.

Considering the variation in interference mitigation, the results showed that the HDW-induced F-OFDM waveform mitigated ACI more effectively than both the HW-induced F-OFDM and HKW-induced FOFDM systems. This simply means that the HDW-F-OFDM waveforms. This behavior indicated that the HDW-induced F-OFDM waveform is more suitable for generating asynchronous waveforms.

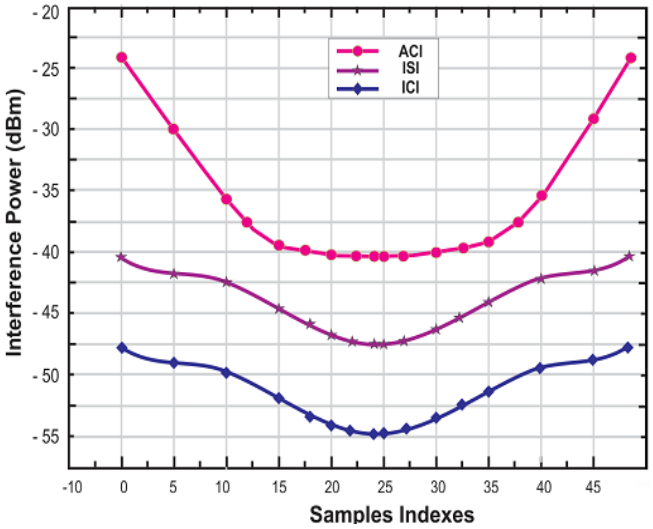


Figure 7. Interference Power Mitigation of HDW-Induced F-OFDM Waveform at 120 kHz SCS.

Table 4
Interference Power Mitigation of HDW-Induced F-OFDM Waveform versus HW-Induced F-OFDM Waveform at 120 kHz SCS

Interference	HW-Induced F-OFDM at 120 kHz SCS	HDW-Induced F-OFDM at 120 kHz SCS	Percentage Improvement
ACI Power (dBm)	-20.55	-30.02	46.08%
ISI Power (dBm)	-32.08	-38.52	20.07%
ICI Power (dBm)	-41.79	-51.17	22.44%

Comparing the results presented in Figures 6 and 7 with those of Figure 5 (b) showed that the HKW-induced F-OFDM and HDW-induced F-OFDM waveforms achieved better interference mitigation than the conventional HW-induced F-OFDM waveform. Likewise, the results demonstrated that both proposed waveforms improved system scalability as the SCS and β were increased. Furthermore, the HKW-induced F-OFDM waveform generated signals that better satisfied the requirements for maintaining orthogonality, whereas the HDW-induced F-OFDM waveform produced signals with improved asynchronous characteristics. Finally, the waveforms generated using the HKW-induced and HDW-induced F-OFDM approaches were demodulated using the FFT to obtain the proposed alternative waveforms that satisfied the AIM requirements for 5G NR FR2 systems.

VI. CONCLUSION AND RECOMMENDATION

In conclusion, this work achieved AIM transmission efficacy using the HKW-induced F-OFDM and HDW-induced F-OFDM waveforms in a CLTF module with an augmented filtering approach. The results showed that the two developed waveforms outperformed the conventional HW-induced F-OFDM waveform in terms of interference mitigation, thereby enabling effective 5G FR2 transmission. The HKW-induced F-OFDM waveform achieved the best ICI and ISI mitigation performance, thereby enabling effective waveform orthogonality. The HDW-induced F-OFDM waveform also achieved better ACI mitigation, making it more suitable for asynchronous waveform applications. At 120 kHz SCS, both the HKW-induced F-OFDM and HDW-induced F-OFDM waveforms performed better than the conventional HW-induced F-OFDM waveform.

The proposed waveforms were implemented using windowing with a non-recursive structure. This approach was adopted because windowing and filtering of conventional multicarrier waveforms are fundamental requirements for designing highly flexible waveforms for 5G NR networks and beyond. In addition, the developed waveforms can be easily designed and implemented in cyclic waveforms because the filter response depends only on the present and past input samples (causality), thereby satisfying the causality requirement.

At the core of this work, the newly developed waveforms effectively addressed the fundamental problems previously observed in conventional multicarrier OFDM designs, including structural, numerical, and physical modeling challenges, particularly within the FR2 frequency range. This finding informed the development of the non-unity CLTF module, which was designed to mitigate these fundamental problems through improved OoBE suppression and PAPR reduction.

Among the areas that require further work are the following recommendations:

i. The hybridization of HKW-induced F-OFDM and HDW-induced F-OFDM waveforms could provide better alternative and adaptive stop-band attenuation, higher steepness, lower side lobes, and improved noise reduction. This is because it combines the advantages of the Hanning, Kaiser, and Dolph windows, although at the expense of increased power consumption. Future research should therefore investigate techniques to mitigate this additional power consumption in the hybridized system to further improve 5G NR wireless system efficiency.
ii. This research was not able to perform simulations beyond 120 kHz SCS because of hardware constraints that resulted in computational difficulties during data iterations. This limitation highlights the need for higher-performance computing systems to enable efficient simulations at higher SCS values and further improve system efficiency.
iii. It was analytically and computationally observed that increasing the SCS at 120 kHz improved interference mitigation network redundancies with further increases in SCS. To address this limitation, more effective technique for utilizing the unused spectrum is required. The hybridization of Software Defined Radio (SDR) and Machine Learning (ML) algorithms may maximize the utilization of these redundant spectra and improve system scalability.

ACKNOWLEDGMENT

The authors wish to acknowledge the Air Force Institute of Technology Kaduna and the Federal University of Applied Sciences Kachia for providing the enabling environments and facilities for the conduct of this research.

CONFLICT OF INTEREST

The authors declare that there is no conflict of interest regarding the publication of the paper.

AUTHOR CONTRIBUTION

All authors contributed equally to the conception and design of the study, data collection and testing, analysis, and manuscript preparation.

REFERENCES

[1] F. Conceição, M. Gomes, V. Silva, R. Dinis, A. Silva, and D. Castanheira, "A Survey of Candidate Waveforms for beyond 5G Systems," Electronics, vol. 10, no. 1, p. 21, Dec. 2020, https://doi.org/10.3390/electronics10010021

[2] Z. Augustine, A. M. Tekanyi, S. M. Sani, A. D. Usman, A. S. Yaro, "Development of a Novel Feedback Filtered Orthogonal Frequency Division Multiplexing Scheme for 5G Network and Beyond," Journal of Telecommunication, Electronic and Computer Engineering (JTEC), vol. 13, no. 4, pp. 1-6, Dec. 2021.

[3] R. Priya and R.K Budania, "Innovative Multi-Band Switchable Microwave Filter for Future Wireless Communication Systems." Cuestiones de Fisioterapia 54.3 (2025): 5248-5254.

[4] L. Zhang, A. Ijaz, P. Xiao, M. M. Molu, and R. Tafazolli, "Filtered OFDM systems, algorithms, and performance analysis for 5G and beyond," IEEE Transactions on Communications, vol. 66, no. 3, pp. 1205–1218, Nov. 2017, https://doi.org/10.1109/tcomm.2017.2771242

[5] H. A. Marzog, H. J. Abd and A. Z. Yonis, "Noise Removal of ECG signal using Multi-Techniques," 2022 IEEE Integrated STEM Education Conference (ISEC), Princeton, NJ, USA, 2022, pp. 397-403, https://doi.org/10.1109/ISEC54952.2022.10025094

[6] G. Chandra, N. Sahu, R. Sahu, and P. K. Rahi. "Design of Low Pass FIR Filter Using Parzen and Nuttall Window Techniques," International Journal for Research in Emerging Science and Technology, vol. 3, no. 8, pp. 11-16, 2016.

[7] A. Z. Yonis and K. K. Mohammed, "Investigation of pattern division multiple access technique in wireless communication networks Indonesian," Journal of Electrical Engineering and Computer Science vol. 26, no. 1, April 2022, pp. 296-303. http://doi.org/10.11591/ijeecs.v26.i1.pp296-303

[8] A. Andrawes, R. Nordin, and N. F. Abdullah, "Energy-Efficient Downlink for Non-Orthogonal Multiple Access with SWIPT under Constrained Throughput," Energies, vol. 13, no. 1, p. 107. 2020. https://doi.org/10.3390/en13010107

[9] Z. Augustine, H. Bello, A. M. S. Tekanyi, A. S. Yaro, H. A. Abdulkareem, O. O. Umeonwuka, U. F. Abdu-Aguye, "Generation of 5G frequency one model based on orthogonal multiple access technique of filtered-orthogonal frequency division multiplexing scheme for advanced interference evaluation," Computers and Electrical Engineering, vol. 128, pp. 110056. Jan. 2025, 1;123:110056.

[10] H. Hong and Z. Li, "Hybrid Adaptive Bias OFDM-Based IM/DD Visible Light Communication System," Photonics, vol. 8, no. 7, p. 257, Jul. 2021, https://doi.org/10.3390/photonics8070257

[11] P. Achimugu, Z. Augustine, M.J. Abdullahi, O. Lanihu, R.E. Yoro, A.A. Abba, and A. Hamisu, "A Survey of Wireless Cellular Network Generations and Their Channel Access Techniques" Journal of Computing and Social Informatics Vol. 5, No. 1, 2026, pp. 1-12. https://doi.org/10.64509/jicn.21.50

[12] A. Kumar and N. P, "OFDM system with cyclostationary feature detection spectrum sensing," ICT Express, vol. 5, no. 1, pp. 21–25, Feb. 2018, https://doi.org/10.1016/j.icte.2018.01.007

[13] S. Natarajan, S.K. Mani, "OFDM implementation of image and video capturing with SD Ram using Artix-7." AIP conference proceedings. Vol. 2857. No. 1. AIP Publishing LLC, 2023. https://doi.org/10.1063/5.0165360

[14] Z. Augustine, A.S. Yaro, A.M.S. Tekanyi, H Bello, U.F. Abdu-Aguye, and EE Agbo,. "Feedback filtered-OFDM waveform candidature for interference mitigation in 5G networks and beyond." International Journal of Integrated Engineering Vol. 17, No. 1, 2025, pp. 323-339. https://doi.org/10.30880/ijie.2025.17.01.027

[15] J. Bai, S. Yuan, Z. Duan. "Research on the Interference Effects of 5G's Key Parameters on Radio Altimeters," Aerospace **2025**, vol. 12, p. 16. https://doi.org/10.3390/aerospace12010016

[16] A. Boruah, N.H. Singh, A. Biswas, S. Majumder, "Enhancing 5G Data Transmission Through Sub-Carrier Spacing Optimization." Engineering Access 11.1 (2025): 24-44.

[17] D.T. Hieu, T. Van Nghia, and N. Le Cuong, "Window-based alternative filters for f-OFDM in next generation wireless communication systems." Journal of Military Science and Technology 87, pp. 9-19, 2023. https://doi.org/10.54939/1859-1043.j.mst.87.2023.9-19

[18] A. Andrawes, R. Nordin, and M. Ismail. "Wireless Energy Harvesting with Cooperative Relaying under the Best Relay Selection Scheme," Energies, vol. 12, no. 5, 892. https://doi.org/10.3390/en12050892

[19] H. Rakshit and M. A. Ullah, "A comparative study on window functions for designing efficient FIR filter," 2014 9th International Forum on Strategic Technology (IFOST), Cox's Bazar, Bangladesh, 2014, pp. 91-96, https://doi.org/10.1109/IFOST.2014.6991079

[20] Z. Augustine, U.F. Abdu-Aguye, A.S. Yaro, H. Bello, A.M.S. Tekanyi, O.O. Umeonwuka, I. Yau, "Wireless multi-carrier transmission techniques for commercial deployment in LTE, LTE-A, and 5G FR1." Journal of Electrical Systems and Information Technology 12.1 (2025): 77. https://doi.org/10.1186/s43067-025-00270-5

[21] S. Bhowmik, M. S. Jahadun-Nobi, R. Chowdhury, O. M. Ali, S. Chowdhury, and M. S. Boby. An Efficient Optimized Window Function for Designing Low Pass FIR Filter. IOSR Journal of Electrical and Electronics Engineering, vol. 15, no. 4. pp. 26-32, 2020. https://doi.org/10.9790/1676-1504012632

[22] M. Yang, Y. Chen and L. Du, "Interference Analysis and Filter Parameters Optimization for Uplink Asynchronous F-OFDM Systems," in IEEE Access, vol. 7, pp. 48356-48370, 2019, https://doi.org/10.1109/ACCESS.2019.2910592

[23] A. Hammoodi, L. Audah, L. Al-Jobouri, M. A. Mohammed, and M. S. Aljumaily, "New 5G Kaiser-Based windowing to reduce out of band emission," Computers, Materials & Continua/Computers, Materials & Continua (Print), vol. 71, no. 2, pp. 2721–2738, Dec. 2021, https://doi.org/10.32604/cmc.2022.020091

[24] R. P. Narwaria and M. Kumar. "Comparison of FIR Filter Using Different Window Functions," International Research Journal of Engineering and Techology . vol. 05, no. 10, pp. 634-637, Oct. 2018.

[25] E. Punskaya. Design of FIR Filter, E. Punskaya. "Design of FIR Filter," University of Oxford, [Online]. Available: https://www.robots.ox.ac.uk/~gari/teaching/cdt/A3/readings/Filtering_and_FFT/3F3_5_Design_of_FIR_Filters.pdf, Accessed: Mar. 24, 2025

[26] H. N. Uzo, O. U. Oparaku, and V. C. Chijindu, "Design of FIR digital filters using Semi-ellipse window," Indonesian Journal of Electrical Engineering and Informatics (IJEEI), vol. 9, no. 3, Sep. 2021, https://doi.org/10.52549/ijeei.v9i3.2481.